Supporting information

High-performance solid-state zinc-ion battery enabled by flexible and high Zn^{2+} conductive solid-polymer electrolyte

Rangaswamy Puttaswamy[a], Zhenchuan Tian[a], Hyocheol Lee[a], Do Youb Kim[b], Anh Le Mong[a], Dukjoon Kim[a*]

[a]School of Chemical Engineering, Sungkyunkwan University, Suwon, Gyeonggi, 16419, Republic of Korea

[b]Energy Materials Research Center, Korea Research Institute of Chemical Technology, 141 Gajeongro, Yuseong, Daejeon 34114, Republic of Korea.

[*] Corresponding author: Professor Dukjoon Kim
Tel.: +82 31 290 7250.
Fax: +82 31 290 7270.
Email address: djkim@skku.edu (D. Kim).

Experimental Section:

Synthesis of PVA-inter-PEG$_{50\%}$/ZnTFS$_{50\%}$, zinc-ionic liquid, PVA-inter-PEG$_{30\%}$/IL$_{70\%}$ and PVA-inter-PEG$_x$/IL$_x$ (x= 60/40, 50/50, and 40/60) SPEs.

Synthesis of PVA-inter-PEG$_{50\%}$/ZnTFS$_{50\%}$: 0.14 g of polyvinyl alcohol (PVA) and 0.06 g of polyethylene glycol diacrylate (PEGDA) with 3 mg of azobisisobutyronitrile (AIBN) were dissolved in 10 ml of N-Methyl-2-pyrrolidone (NMP) solvent with vigorous stirring at room temperature. After 10 mins, 0.2 g of $Zn(CF_3SO_3)_2$ (ZnTFS) salt is slowly added to the solution and stirred well at room temperature for 24 h. After 24 h of vigorous stirring, the solution was transferred to a Teflon dish, and heated at 80 °C for 24 h under a vacuum to remove any residual NMP solvent. The resulting polymer is abbreviated as *PVA-inter-PEG$_{50\%}$/ZnTFS$_{50\%}$* {50% (0.14g PVA+ 0.06 g PEGDA= 0.2 g) and 50% (0.2 g ZnTFS) = total of 100% (0.4 g)}.

Synthesis of zinc-ionic liquid: Zinc ionic-liquid (IL) electrolyte was prepared by dissolving 3.635 g ZnTFS salt into 10 ml of 1-ethyl-3-methylimidazolium trifluoromethanesulfonate (EMIM Otf) at 60 ℃ with vigorous stirring for 24 h. The transparent zinc IL was achieved after the solution was cooled at ambient temperature.

Synthesis of PVA-inter-PEG$_{30\%}$/IL$_{70\%}$: 0.084 g of PVA and 0.036 g of PEGDA with 1.8 mg AIBN are dissolved into 10 ml of NMP solvent with vigorous stirring at room temperature. After 10 mins, 0.28 g of zinc ionic-liquid (EMIM Otf + ZnTFS) is added to the solution and stirred well at room temperature for 24 h (**Scheme S1**). After 24 h of vigorous stirring, the solution was transferred to a Teflon dish, and heated at 80 ℃ for 24 h under a vacuum to remove any residual NMP solvent. The resulting polymer electrolyte is abbreviated as PVA-inter-PEG$_{30\%}$/IL$_{70\%}$ {30% (0.084g PVA+ 0.036 g PEGDA= 0.12 g) and 70% (0.28 g zinc ionic-liquid) = total of 100% (0.4 g)}.

Similarly, the synthesis of PVA-inter-PEG_x/IL_x (x= 60/40, 50/50, and 40/60) SPEs was carried out by varying the PVA, PEGDA, AIBN, and zinc-ionic liquid. The detailed synthetic scheme of synthesis is provided in Table S1.

Table S1: Synthesis of PVA-inter-PEG_x/IL_x (x= 60/40, 50/50, and 40/60) SPEs.

PVA	PEGDA	Total weight of PVA and PEGDA (ratio)	AIBN	Zinc-ionic liquid (ratio)	PVA-inter PEG:Zinc-ionic liquid ratio	Abbreviations
0.168 g	0.072g	0.24 g (60 %)	3.6 mg	0.16 g (40 %)	60/40	PVA-inter-$PEG_{60\%}/IL_{40\%}$
0.14 g	*0.06 g*	0.20 g (50 %)	3.0 mg	0.20 g (50 %)	50/50	PVA-inter-$PEG_{50\%}/IL_{50\%}$
0.112 g	*0.048 g*	0.16 g (40 %)	2.4 mg	0.24 g (60 %)	40/60	PVA-inter-$PEG_{40\%}/IL_{60\%}$

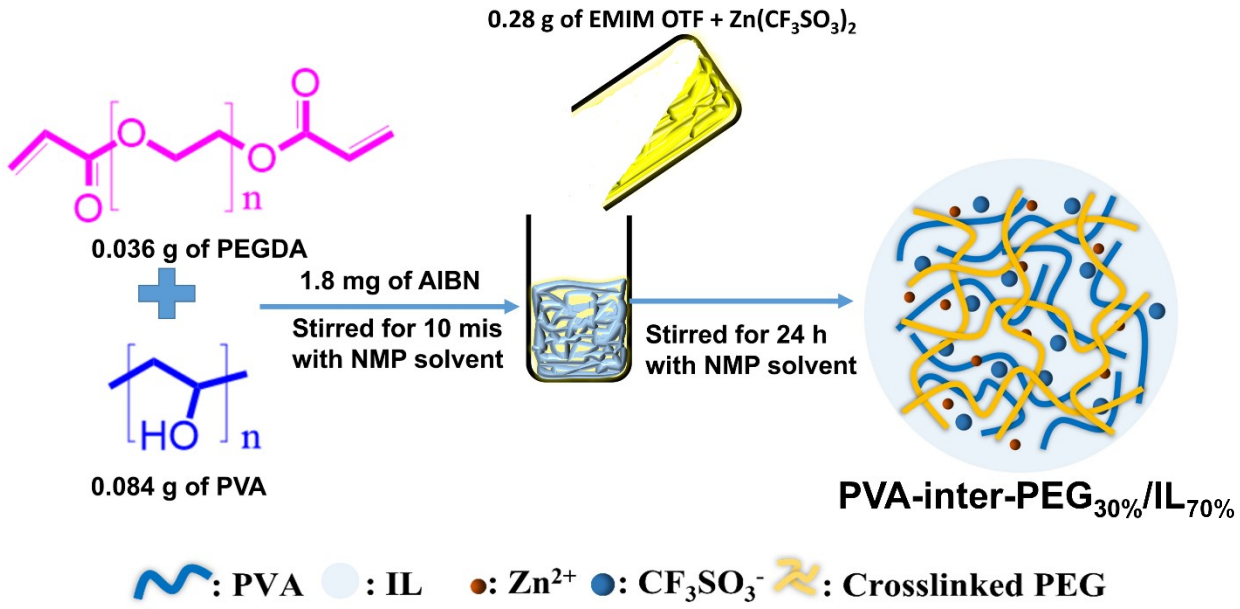

Scheme S1: Synthesis schematic of the PVA-inter-$PEG_{30\%}/IL_{70\%}$ SPE.

Synthesis of $V_{10}O_{24}.nH_2O$: The synthesis of $V_{10}O_{24}.nH_2O$ is carried out according to the reported procedure[1] with slight modifications. In brief, 2.0 g of commercial V_2O_5 powder and 2 g of glucose

were added to 80 ml distilled H_2O, and then the mixture was subjected to reflux at 100 °C for 15 h in an oil bath by vigorous stirring to achieve the dark blue color from a yellow dispersion (**Fig. S2**). The product was washed with water and ethanol mixture 5 times and dried at 70 °C for 10 h.

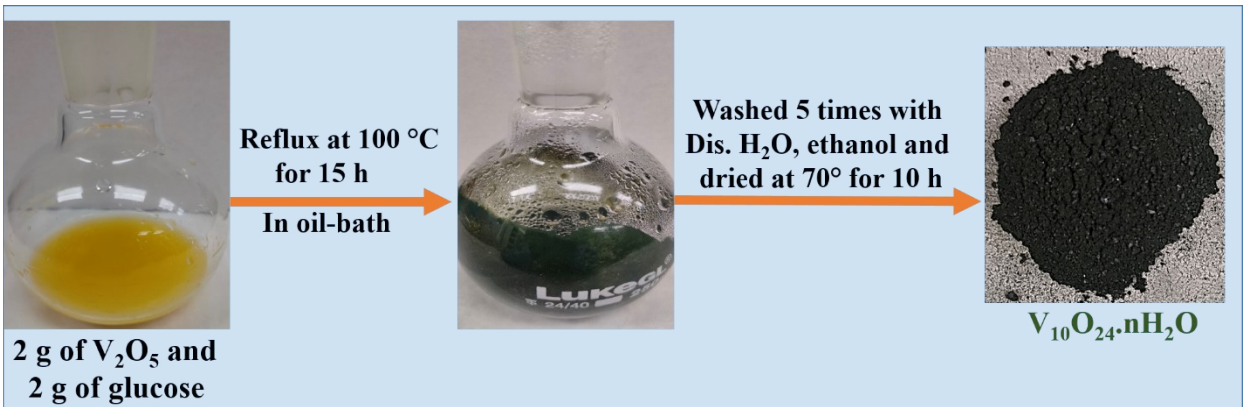

Scheme S2: Synthesis of $V_{10}O_{24}.nH_2O$ cathode material.

Materials characterizations: The Powder X-ray diffraction (XRD) patterns were recorded using Bruker D-8 Advance diffractometer operated at a voltage of 40 kV and a current of 40 mA using Cu Kα (1.5418 Å) as the X-ray source at a scan rate of 3º/min. Raman spectra were recorded using Bruker (SENTERRA Raman, A670 HYPERION) spectrometer. The thermal degradation of the materials was evaluated by thermogravimetric analysis (TGA) (TGA2050, TA instruments, New Castle, USA) at a heating rate of 10 °C min^{-1} under N_2 gas. The surface area and pore properties of the $V_{10}O_{24}.nH_2O$ were carried out by Brunauer-Emmett-Teller (BET); N_2 adsorption-desorption studies using Micrometrics ASAP-2010 automatic specific surface area and porous physical adsorption analyzer. The morphological information was obtained from scanning electron microscope (FE-SEM) (JEOL JSM7600F, Japan), equipped with energy-dispersive X-ray spectroscopy (EDS). Transmission electron microscopy (TEM) images were obtained using JEOL, JEM-2100F operating at 200 kV. Energy-dispersive X-ray spectroscopy (EDX) was carried out by

using Oxford INCA system, Oxford, UK. Fourier-transform infrared spectroscopy (FTIR, Tensor 27, Bruker, Germany) of the samples were collected at a resolution of 2 cm^{-1} in the spectral range from 4000-500 cm^{-1}. Differential scanning calorimetry (DSC) (TAQ2000, TA instrument, Milford, MA, USA) was investigated for analyzing the crystalline/amorphous phase transitions of SPEs from -40 °C to 60 °C. A universal tensile machine (UTM) (Lloyd instrument, USA) was applied to investigate the stress-strain behavior of SPE membranes.

Electrochemical measurements: Alternating current (AC) electrochemical impedance spectroscopy (EIS, Biologic, France) was used to investigate the Zn^{2+} conductivity of PVA-inter-PEG_x/IL_x based SPEs under 5 mV in the scanning frequency range from 10^6 to 1 Hz for the symmetric strain steel cells (SS/SPE/SS). The following eq (1) was applied for calculating Zn^{2+} conductivity: $\sigma = \frac{D}{R \times A}$ …….....…….(1)

Where A and D are the area and thickness of SPEs, respectively, the bulk resistance (R) was obtained from the Nyquist plots. AC EIS was also applied to determine the interfacial resistance between zinc foil and SPEs at 5 mV and the scanning frequency of 10^6 Hz to 1 Hz. Linear sweep voltammetry (LSV) was performed at a scan rate of 0.1 mV s^{-1} to determine the electrochemical stability window of SPEs by pairing them with zinc foil and stainless-steel electrode. Galvanostatic stripping/plating analysis of Zn symmetric cells (Zn/SPE/Zn) was carried out at a fixed charging/discharging time of 1 h with different current densities (0.2, 0.4, 0.6, 0.8, and 1.0 mA cm^{-2}), and also long-term Zn stripping/plating analysis was carried out at 0.2 mA cm^{-2} over 1500 h.

The cathodes were prepared by mixing the $V_{10}O_{24}.nH_2O$, carbon black and polyvinylidene fluoride (PVDF) in the ratio of 70:20:10 wt% with a few drops of NMP, then cast onto carbon paper (GDL) and dried in an oven at 80 ºC for 10-12 h. The electrochemical measurements were evaluated by 2032-coin cells type wherein zinc foil (0.25 mm thickness, Alfa Aesar) was used as

an anode and PVA-inter-$PEG_{30\%}/IL_{70\%}$ as SPE. Approximately 2 mg cm^{-2} of active materials were maintained for the complete ZIB study. All electrochemical performances were evaluated using Biologic Potentiostat, and all the electrochemical studies were conducted at room temperature.

Results and discussions

***FT-IR and XRD of* PVA-inter-$PEG_{30\%}/IL_{70\%}$**

The chemical cross-linking reaction and amorphous nature of PVA-inter-$PEG_{30\%}/IL_{70\%}$ are validated by FT-IR and XRD analysis, respectively. In FT-IR analysis (**Fig. S1a**), the PEGDA precursor showed an IR band at 1640 cm^{-1} corresponding to C=C bond stretching of methacrylate.[2, 3] The completely or mostly disappeared C=C stretching in PVA-inter-$PEG_{30\%}/IL_{70\%}$ SPE indicates the successful free radical polymerization of the PEGDA molecules (full conversion of PEGDA monomer by reactions).[2, 4, 5] The vibration bands at 1720 cm^{-1} correspond to the C=O stretching of crosslinked PEG.[2] In XRD patterns (**Fig. S1b**), the as-prepared PVA-inter-$PEG_{30\%}/IL_{70\%}$ SPE shows a broad scattering around 2θ = ~19.5° with reduced intensity. Therefore, the broad XRD patterns with reduced peak intensity suggest the formation of the amorphous phase of the PVA-inter-$PEG_{30\%}/IL_{70\%}$ SPE. This amorphous nature of PVA-inter-$PEG_{30\%}/IL_{70\%}$ SPE induces high Zn^{2+} concentration for conduction. However, the XRD patterns of pure PVA and $Zn(CF_3SO_3)_2$ salt suggest semi-crystalline and pure crystalline in nature, respectively. The semi-crystalline nature of PVA restricts its polymer segmental motion for Zn^{2+} transport.

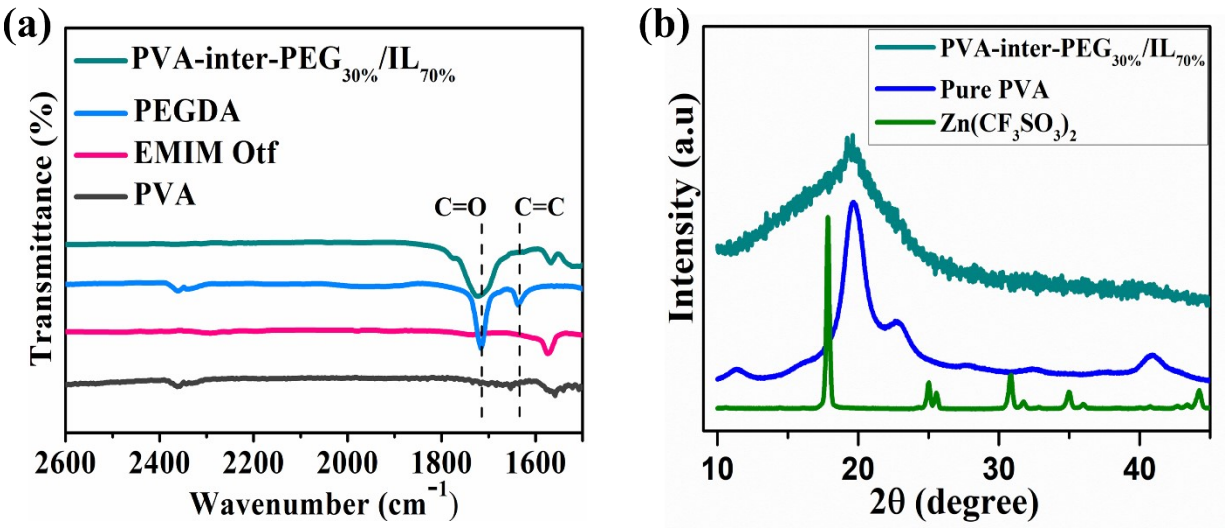

Fig. S1: (a) FTIR spectra of pure PVA, EMIM Otf IL, PEGDA, and PVA-inter-$PEG_{30\%}/IL_{70\%}$ SPE. (b) XRD pattern of PVA, $Zn(CF_3SO_3)_2$ salt and PVA-inter-$PEG_{30\%}/IL_{70\%}$ SPE.

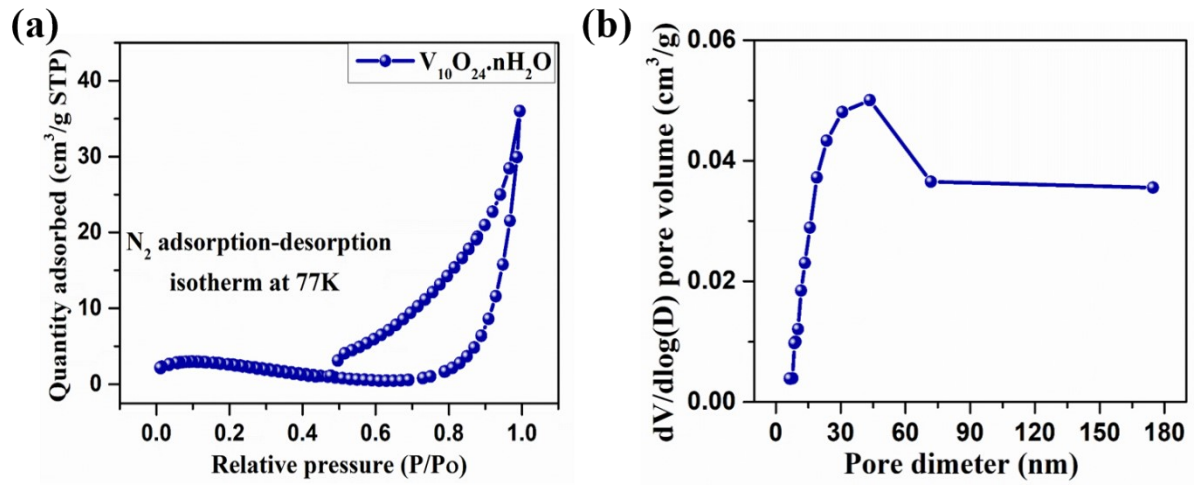

Fig. S2: (a) BET adsorption/desorption isotherms, and (b) BJH pore size distribution plots of $V_{10}O_{24}.nH_2O$ cathode material.

Table S2: Average particles size, BET surface area, Langmuir surface area, BJH adsorption average pore diameter, and t-plot microporous area of $V_{10}O_{24}.nH_2O$ cathode material.

	Average particles size	**BET surface area ($m^2 g^{-1}$)**	**Langmuir surface Area ($m^2 g^{-1}$)**	**BJH adsorption average pore diameter (4V/A)**	**t-plot micropore Area ($m^2 g^{-1}$)**
$V_{10}O_{24}.nH_2O$	937.86 nm	6.397	10.07	32.5530 nm	16.8711

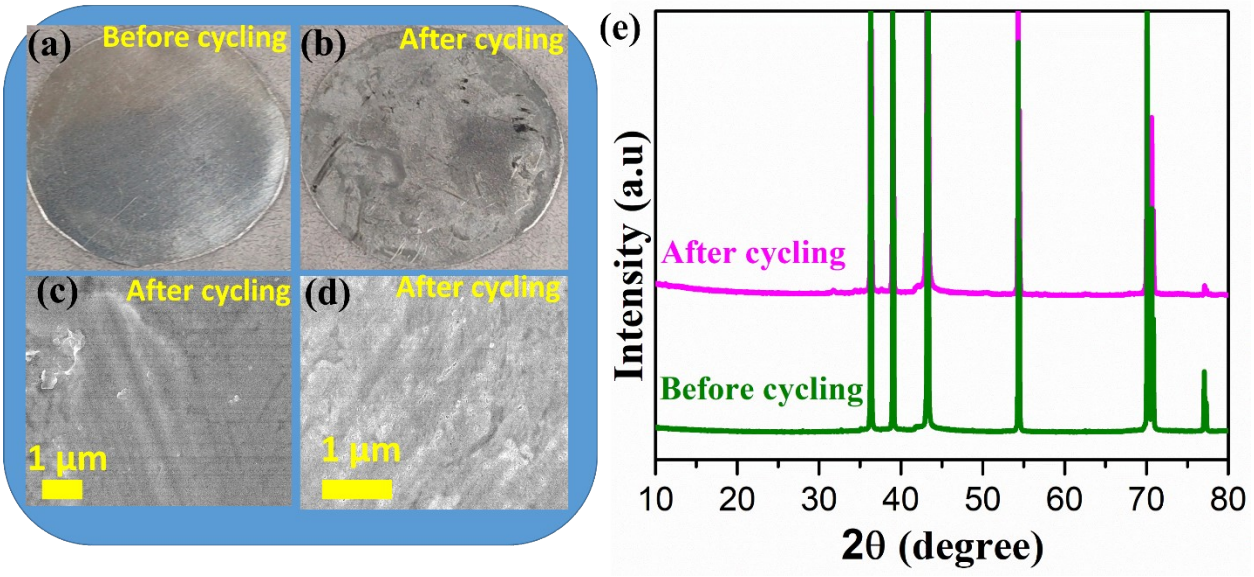

Fig. S3: (a) Photographs of zinc surface taken before, and (b) after 700 h of stripping/plating cycles. (c and d) FESEM images of zinc anode surface taken after 700 h of stripping/plating cycles. (e) XRD patterns of zinc foil before, and after 700 h of stripping/plating cycles.

Table S3: Comparison of Zn^{2+} conductivity, tensile strength, oxidative stability window, and stripping/plating cyclic hours of PVA-inter-$PEG_{30\%}/IL_{70\%}$ SPE with recently reported solid-state electrolytes for ZIB applications.

Electrolyte composition	**Zn^{2+} conductivity (mS cm^{-1})**	**Tensile strength (MPa)**	**Oxidative stability window (V)**	**Striping/plating cyclic hours**	**References**
Hbimcp/PPO/$Zn(CF_3SO_3)_2$	0.01	1.0	1.90	200 h	[6]
CMC/PNiPAM/ $Zn(CF_3SO_3)_2$	0.16	37.9	/	150 h	[7]
PVDF-HFP/ $Zn(CF_3SO_3)_2$	0.02	8.0	1.70	100 h	[8]
PVHF/MXene-g-PMA0.05/ $Zn(CF_3SO_3)_2$	0.27	13.0	2.79	1200 h	[9]
DOL/ $Zn(BF_4)_2$	19.60	/	2.61	1800 h	[10]
PVA/PEG/EMIM Otf/ $Zn(CF_3SO_3)_2$	**~2.26**	**~1.2**	**~2.8**	**3000 h**	**Present work**

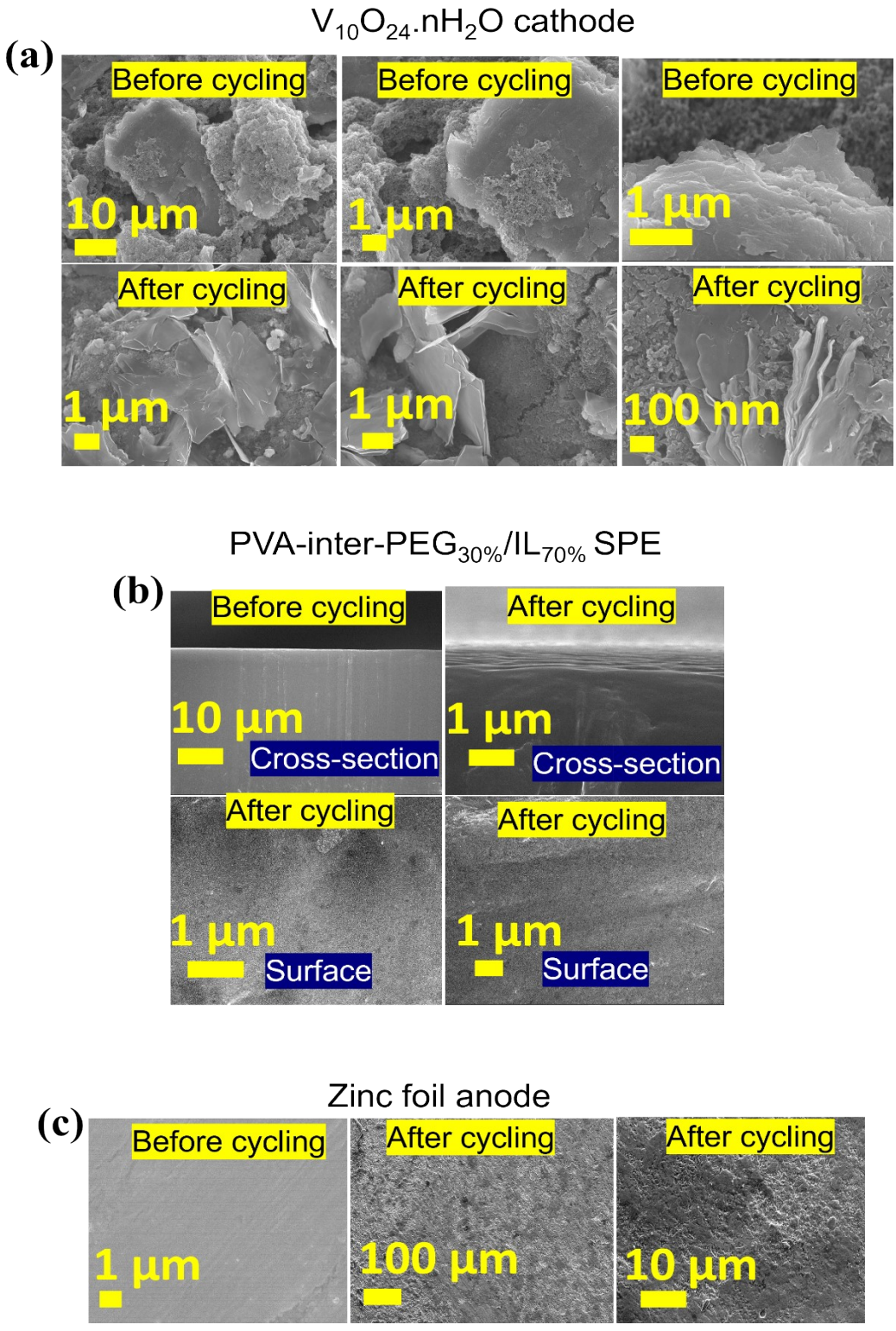

Fig. S4: FESEM images of (a) $V_{10}O_{24}.nH_2O$ cathode, (b) PVA-inter-$PEG_{30\%}/IL_{70\%}$ SPE and (c) zinc foil before and after 4000th charge/discharge cycles at 10 A g^{-1}.

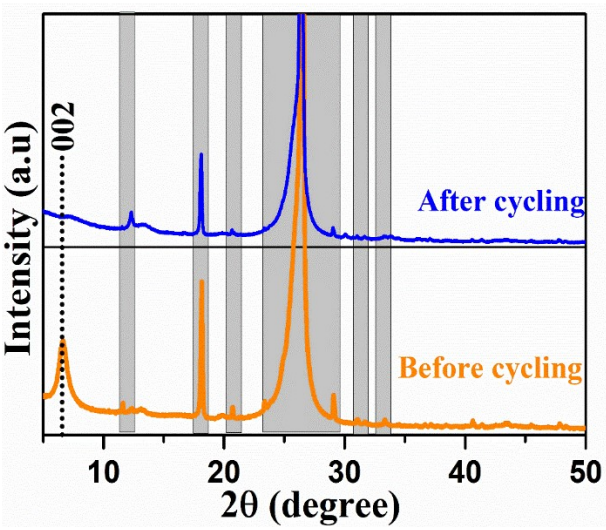

Fig. S5: XRD patterns of $V_{10}O_{24}.nH_2O$ taken before and after 4000 cycles at 10 A g^{-1}.

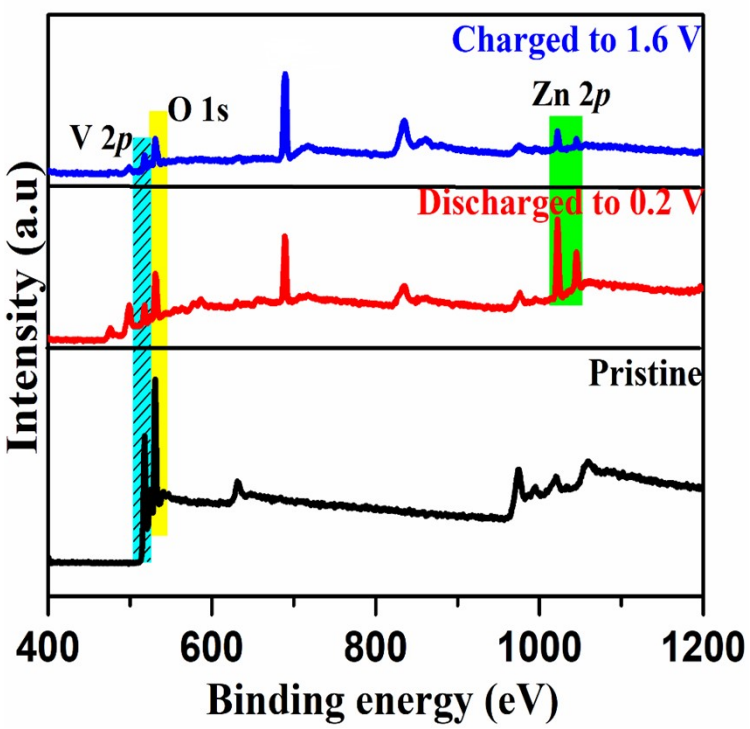

Fig. S6: The survey XPS spectrum of pristine, fully discharged, and fully charged $V_{10}O_{24}.nH_2O$ cathode material.

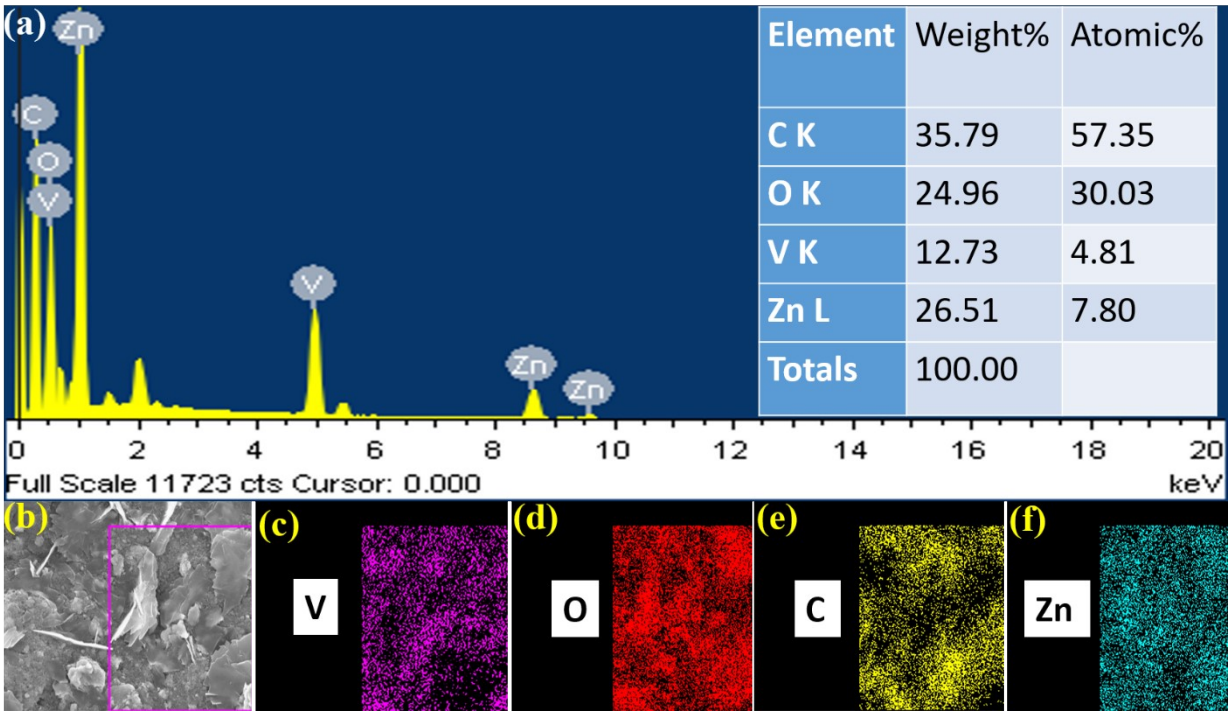

Fig. S7: (a) EDX profile of $V_{10}O_{24}.nH_2O$ after fully discharged to 0.2 V. EDX mapping images (Fig. S7c-f) showing the presence of V, O, C, and Zn (Fig. S7c-f mapping images are obtained from Fig. S7b).

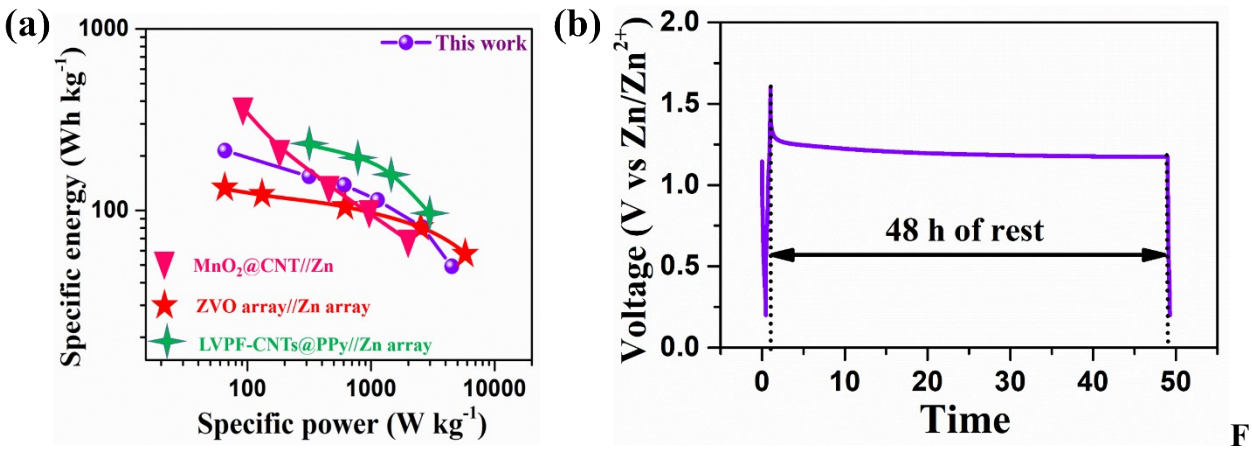

ig. S8: (a) Ragone plot, and (b) self-discharge performance of SS Zn//$V_{10}O_{24}.nH_2O$ cell (the cell first charged at 0.5 A g^{-1} and rested for 48 h).

Fig. S8(a and b) shows the Ragone plot, and self-discharge profile of SS Zn//$V_{10}O_{24}.nH_2O$ cell assembled with PVA-inter-$PEG_{30\%}/IL_{70\%}$ SPE. The energy and power densities of $V_{10}O_{24}.nH_2O$ were calculated from the data illustrated in **Fig. S8a**, and the corresponding results were compared with the reported SPE based RZIBs.[11-13] The SS Zn//$V_{10}O_{24}.nH_2O$ cell with PVA-inter-$PEG_{30\%}/IL_{70\%}$ SPE achieved energy density/power density of 213.29 Wh kg^{-1}/65.5 W kg^{-1} (calculated based on the mass of $V_{10}O_{24}.nH_2O$ in the cathode)**.** The self-discharge study (**Fig. S8b**) was carried out for the SS Zn//$V_{10}O_{24}.nH_2O$ cell. After charging the SS Zn//$V_{10}O_{24}.nH_2O$ cell to 1.6 V at 0.5 A g^{-1}, the voltage drop was measured over a resting period of 48 h. SS Zn//$V_{10}O_{24}.nH_2O$ cell in PVA-inter-$PEG_{30\%}/IL_{70\%}$ SPE shows a linear voltage drop up to 1.48 V, and thereafter stable voltage plateau is maintained up to 1.17 V for 48 h. After 48 h resting period, the voltage drop of SS Zn//$V_{10}O_{24}.nH_2O$ cell was found to be 73.12%. This low self-discharge property of Zn//$V_{10}O_{24}.nH_2O$ cell indicates a stable and compatible battery system with PVA-inter-$PEG_{30\%}/IL_{70\%}$ SPE.

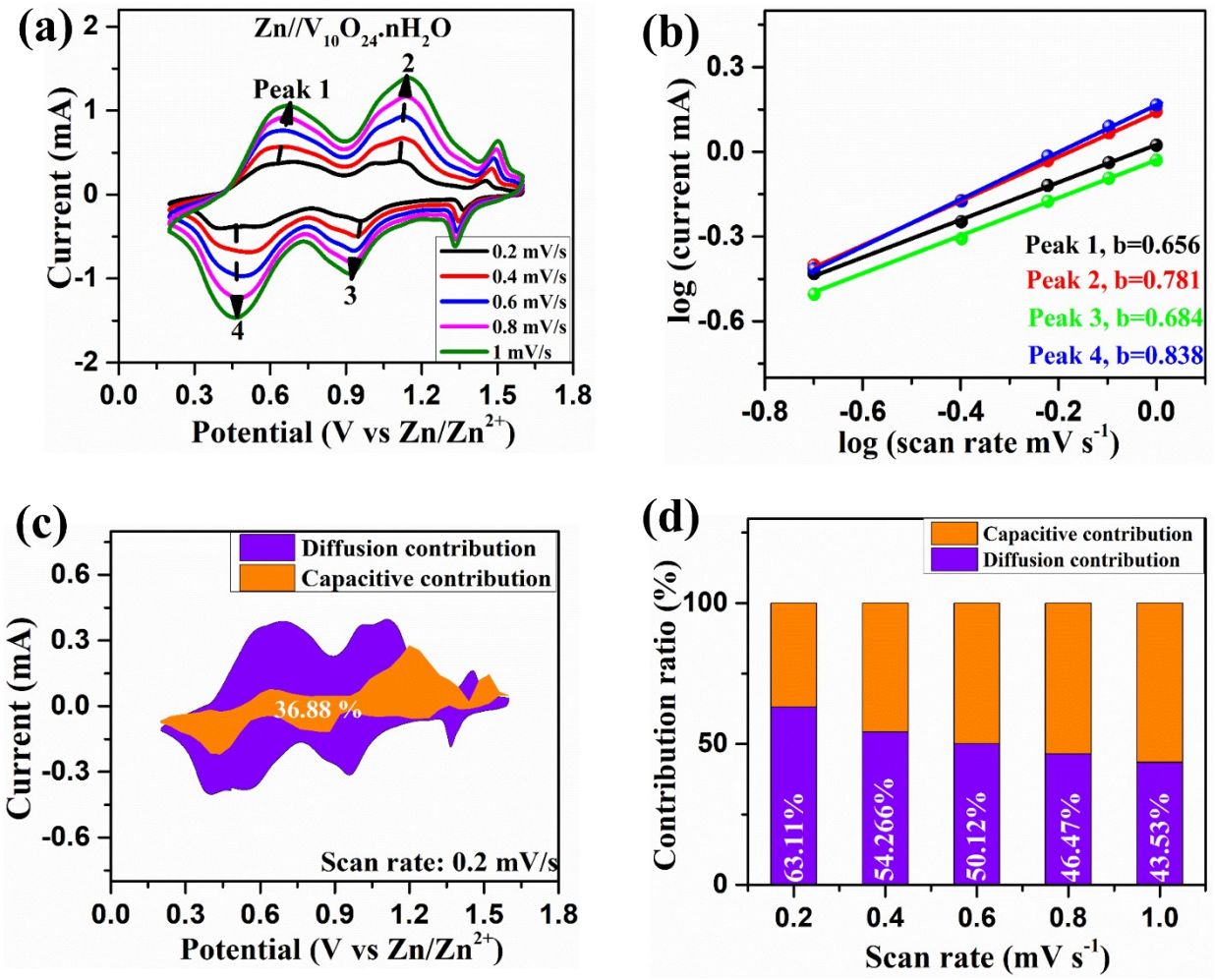

Fig. S9: Charge-storage kinetic studies of SS Zn//$V_{10}O_{24}.nH_2O$ cell fabricated with PVA-inter-$PEG_{30\%}/IL_{70\%}$ SPE. (a) Cyclic voltammetry plots at different scan rates from 0.2 to 1 mV s^{-1}. (b) log of peak current obtained from the CV plots at different scan rates vs log of scan rate plots. (c) Separation of the capacitive currents (k_1v) and diffusion currents ($k_2v^{1/2}$) at a scan rate of 0.2 mV s^{-1}, and (d) column graphs of contribution ratio of the diffusion and capacitive charge as a function of scan rate.

The intrinsic charge storage kinetics was analyzed for the SS Zn//$V_{10}O_{24}.nH_2O$ cell assembled with PVA-inter-$PEG_{30\%}/IL_{70\%}$ SPE to investigate the contribution of diffusion and pseudocapacitive processes to the total charge. The charge storage kinetics was studied from the CV plots at different scan rates (0.2 to 1 mV s^{-1}) (**Fig. S9a**). When the scan rate increased, the peak intensity gradually increased with noticeable displacement due to the polarization effect of the electrode.[14, 15] By connecting the vertices of redox peaks in the five curves, four straight lines are drawn as shown in **Fig. S9b**. The quantitative relation between the scan rate (ν) and peak current (*i*) can be obtained from the following equation.

$$i=av^b \text{ or } \log(i)= \log(a) + b \log(v) \quad \text{.....(1)}$$

where "*i*" indicates current, "*a*" and "*b*" are adjustable parameters, and "ν" signifies scan rate (mV s^{-1}). The value of "*b*" calculated from the log "*i*" against the log "ν" plot, basically represents the nature of storage which can be regulated by either or both diffusion-controlled and surface-control processes. The value of "*b*" varies between 0.5 and 1.0, where the "*b*" values of 0.5 and 1 imply the ideal diffusion process controlled by ion intercalation into the electrode bulk and the ideal capacitive process at the electrode interface, respectively.[16-18] According to **Fig. S9b,** the linear fit of the logarithmic relationship between scan rate (ν) and peak current (*i*) shows that slopes of both cathodic and anodic peaks were found to be 0.656, 0.781, 0.684, and 0.838, suggesting that the diffusion and capacitive contribution co-control the charge storage process.

The ratio of diffusion and pseudocapacitive contribution to total capacity was quantitatively separated into the capacitive (k_1v) and diffusion process ($k_2v^{1/2}$) from the current response (*i*) at a specific potential (V) as follows.[19-21]

$$i(V)=k_1v+k_2v^{1/2} \quad \text{.....(2)}$$

Where k_1 and k_2 are the constants at a particular potential irrespective of the scan rate determined from the slopes and intercept of the linear plots using equation (2). **Fig. S9c** displays the capacitive current (k_1) plotted from the typical CV profile at a scan rate of 0.2 mV s^{-1} where the capacitive contribution fraction in the total capacity was estimated to be 36.89% (based on the orange shaded area), while 63.11% was achieved from a diffusion-controlled process. At 1 mV s^{-1}scan rate, however, the capacitive contribution increased to 56.46% (**Fig. S9d**). This result indicates that while the diffusion process dominates the charge storage at low scan rates, the capacitive process gradually increases and dominates the charge storage with increasing scan rate.

Overall, SS Zn//$V_{10}O_{24}.nH_2O$ with PVA-inter-$PEG_{30\%}/IL_{70\%}$ SPE demonstrated better electrochemical performance in comparison to the previously reported cathode materials fabricated with solid-polymer, quasi-solid-state, and hydrogel-based electrolytes (**Table S4**).

Table S4: Comparison of electrochemical performance of $V_{10}O_{24}.nH_2O$ in SPE with reported cathode materials with gel electrolyte, quasi-solid state and solid-state electrolyte.

Anode//cathode	Electrolyte	Battery type	Capacity (mAh g^{-1})	Rate capability	Cycling performance	Energy density	References
LiVPO4F-CNTs@PPY	Acrylamide/APS/methylene bisacrylamide/LiTFSI/Zn(OTf)$_2$	Hydrogel type	146.9 at 0.2 A g^{-1}	146.9/67.1 mAh g^{-1} at 0.2/2.0 A g^{-1}, respectively	87.2% capacity retention after 600 cycles at 1 A g^{-1}	235.6 W h/kg	[11]
Zn@CC//poly(aniline-co-azure C)@C	PVA/NH_4Cl/$ZnCl_2$	Quasi-solid-state	241.4 at 0.8 0.22 A g^{-1}	241.4/81.2 mAh g^{-1} at 0.22/1.33 A g^{-1}, respectively	68% capacity retention after 1000 cycles at 2 mA cm^{-2}	289.3 W h/kg	[22]
Zn@carbon cloth// MnO_2@rGO	Kappa carrageenan/ $ZnSO_4$/$MnSO_4$	Quasi-solid-state	291.5 at 0.15 A g^{-1}	291.5/120 mAh g^{-1} at 0.15/6 A g^{-1}, respectively	80% capacity retention after 450 cycles at 6 A g^{-1}	400 W h/kg	[23]
Zn//NiCo	PANa/KOH/Zn$(CH_3COO)_2$	Hydrogel type	108 at 1.9 C rate	130/100 mAh g^{-1} at 9/36 C rate, respectively	87% capacity retention after 10000 cycles at 19 C rate	172 W h/kg	[24]
Zn//α-MnO_2@CNT	PAM/gelatin/PAN	Solid-state	306 at 61.6 m A g^{-1}	282/150 mAh g^{-1} at 308/1848 mA g^{-1}, respectively	97% capacity retention after 1000 cycles at 2772 mA g^{-1}	6.18 mW h cm^{-2}	[25]
Zn//PANI	PVA/Zn$(CF_3SO_3)_2$	Hydrogel	123 at 0.1 A g^{-1}	123/94 mAh g^{-1} at 0.1/3 A g^{-1}, respectively	97.1% capacity retention after 1000 cycles at 1 A g^{-1}	–	[26]
Zn//MnO_2@CNT-30	ZnTFS-0.2M $MnCl_2$-PVA gel electrolyte	Gel electrolyte	290 at 0.1 A g^{-1}	290/51 mAh g^{-1} at 0.1/2 A g^{-1}, respectively	75% capacity retention after 300 cycles	360 Wh/kg	[12]
Zn//N-ZMO NTAs	(PVA)-LiCl–$ZnCl_2$-$MnSO_4$	Quasi-solid-state	223 at 0.1 A g^{-1}	223/133.3 mAh g^{-1} at 0.1/4 A g^{-1}, respectively	92.1% capacity retention after 1500 cycles at 2 A g^{-1}	214.6 Wh/kg	[27]

Zn//V_2O_5	PVA-$Zn(CF_3SO_3)_2$-TiO_2	Gel electrolyte	255.9 at 50 mA g^{-1}	255.9/124.4 mAh g^{-1} at 50/1000 mA g^{-1}	_	_	28
Zn//$V_{10}O_{24}.nH_2O$	PVA-inter-$PEG_{30\%}/IL_{70\%}$	Solid-state	325.64 at 0.1 A g^{-1}	325/110 mAh g^{-1} at 0.1/10 A g^{-1}, respectively	82.92%, 68.50%, 60.74%, and 57% capacity retention after 1000, 2000, 3000 and 4000 cycles at 10 A g^{-1}, respectively	213.29 W h/kg	**Present work**

References

1. l. Qian, T. Wei, K. Ma, G. Yang and C. Wang, *ACS Applied Materials & Interfaces*, 2019, **11**, 20888-20894.
2. Y. Zhang, W. Lu, L. Cong, J. Liu, L. Sun, A. Mauger, C. M. Julien, H. Xie and J. Liu, *Journal of Power Sources*, 2019, **420**, 63-72.
3. D. K. Wang, S. Varanasi, P. M. Fredericks, D. J. T. Hill, A. L. Symons, A. K. Whittaker and F. Rasoul, *Journal of Polymer Science Part A: Polymer Chemistry*, 2013, **51**, 5163-5176.
4. G. Tan, Y. Wang, J. Li and S. Zhang, *Polymer Bulletin*, 2008, **61**, 91-98.
5. Z. Tian and D. Kim, *Energy Storage Materials*, 2022, **53**, 264-272.
6. D. Liu, Z. Tang, L. Luo, W. Yang, Y. Liu, Z. Shen and X.-H. Fan, *ACS Applied Materials & Interfaces*, 2021, **13**, 36320-36329.
7. I. Dueramae, M. Okhawilai, P. Kasemsiri, H. Uyama and R. Kita, *Scientific Reports*, 2020, **10**, 12587.
8. J. Liu, Z. Khanam, R. Muchakayala and S. Song, *Journal of Materials Science: Materials in Electronics*, 2020, **31**, 6160-6173.
9. Z. Chen, X. Li, D. Wang, Q. Yang, L. Ma, Z. Huang, G. Liang, A. Chen, Y. Guo, B. Dong, X. Huang, C. Yang and C. Zhi, *Energy & Environmental Science*, 2021, **14**, 3492-3501.
10. L. Ma, S. Chen, X. Li, A. Chen, B. Dong and C. Zhi, *Angewandte Chemie*, 2020, **132**, 24044-24052.
11. Z. Liu, Q. Yang, D. Wang, G. Liang, Y. Zhu, F. Mo, Z. Huang, X. Li, L. Ma, T. Tang, Z. Lu and C. Zhi, *Advanced Energy Materials*, 2019, **9**, 1902473.
12. K. Wang, X. Zhang, J. Han, X. Zhang, X. Sun, C. Li, W. Liu, Q. Li and Y. Ma, *ACS Applied Materials & Interfaces*, 2018, **10**, 24573-24582.
13. D. Chao, C. R. Zhu, M. Song, P. Liang, X. Zhang, N. H. Tiep, H. Zhao, J. Wang, R. Wang, H. Zhang and H. J. Fan, *Advanced Materials*, 2018, **30**, 1803181.
14. D. Kundu, P. Oberholzer, C. Glaros, A. Bouzid, E. Tervoort, A. Pasquarello and M. Niederberger, *Chemistry of Materials*, 2018, **30**, 3874-3881.
15. C. Liu, Z. Neale, J. Zheng, X. Jia, J. Huang, M. Yan, M. Tian, M. Wang, J. Yang and G. Cao, *Energy & Environmental Science*, 2019, **12**, 2273-2285.
16. H. Zhao, Q. Fu, D. Yang, A. Sarapulova, Q. Pang, Y. Meng, L. Wei, H. Ehrenberg, Y. Wei, C. Wang and G. Chen, *ACS Nano*, 2020, **14**, 11809-11820.
17. S. Li, X. Wei, C. Wu, B. Zhang, S. Wu and Z. Lin, *ACS Applied Energy Materials*, 2021, **4**, 4208-4216.
18. Y. Liu, Q. Li, K. Ma, G. Yang and C. Wang, *ACS Nano*, 2019, **13**, 12081-12089.
19. J. Feng, Y. Wang, S. Liu, S. Chen, N. Wen, X. Zeng, Y. Dong, C. Huang, Q. Kuang and Y. Zhao, *ACS Applied Materials & Interfaces*, 2020, **12**, 24726-24736.
20. P. He, Y. Quan, X. Xu, M. Yan, W. Yang, Q. An, L. He and L. Mai, *Small*, 2017, **13**, 1702551.
21. R. Puttaswamy, H. K. Beere, P. Yadav, M. Jalalah, M. Faisal, F. A. Harraz and D. Ghosh, *ACS Applied Energy Materials*, 2022, **5**, 8292-8303.
22. P. Li, Z. Fang, Y. Zhang, C. Mo, X. Hu, J. Jian, S. Wang and D. Yu, *Journal of Materials Chemistry A*, 2019, **7**, 17292-17298.
23. Y. Huang, J. Liu, J. Zhang, S. Jin, Y. Jiang, S. Zhang, Z. Li, C. Zhi, G. Du and H. Zhou, *RSC Advances*, 2019, **9**, 16313-16319.

24. H. Wang, J. Liu, J. Wang, M. Hu, Y. Feng, P. Wang, Y. Wang, N. Nie, J. Zhang, H. Chen, Q. Yuan, J. Wu and Y. Huang, *ACS Applied Materials & Interfaces*, 2018, **11**, 49-55.
25. H. Li, C. Han, Y. Huang, Y. Huang, M. Zhu, Z. Pei, Q. Xue, Z. Wang, Z. Liu, Z. Tang, Y. Wang, F. Kang, B. Li and C. Zhi, *Energy & Environmental Science*, 2018, **11**, 941-951.
26. S. Huang, F. Wan, S. Bi, J. Zhu, Z. Niu and J. Chen, *Angewandte Chemie*, 2019, **131**, 4357-4361.
27. W. Qiu, H. Xiao, H. Feng, Z. Lin, H. Gao, W. He and X. Lu, *Chemical Engineering Journal*, 2021, **422**, 129890.
28. C. Liu, Y. Tian, Y. An, Q. Yang, S. Xiong, J. Feng and Y. Qian, *Chemical Engineering Journal*, 2022, **430**, 132748.